Journal of Advances in Science and Technology
Vol. 18, Issue No. 2, September–2021, ISSN 2230-9659

Structural Transformation of Nickel Doped Zinc Oxide Nanostructures

Deepak Chaurasiya[1]*, Dr. Satish Kumar[2]

[1] Research Scholar, Shri Krishna University, Chhatarpur M.P.

[2] Professor, Shri Krishna University, Chhatarpur M.P.

Abstract - ZnO nanoparticles, both undoped and doped with transition metals (Mn, Mg, and Cr), were successfully mass-produced using a simple chemical precipitation technique. Doped ZnO nanoparticles with Mn, Mg, and Cr have already been investigated for their structural, optical, and electrical properties. Recent years have also seen extensive research into nanoscale ferromagnetic Ni/Fe nanoparticles due to the system's tremendous interest in a variety of applications, including storage devices, catalysis, multilayer capacitors, and medical diagnostics as biosensors. Ni+ vacancies, which are monovalent cations, may be introduced into nanostructured NiO to improve the material's ac conductivity by as much as six to eight orders of magnitude, which is great for solar cell applications.

Keywords - Structural Transformation, Nickel, Doped, Zinc Oxide, Nanostructures, etc.

----------X----------

INTRODUCTION

Nanostructured zinc oxide with nickel atoms inserted into it undergoes a structural change that is documented. It is by chemical precipitation that 1-10% nickel-doped ZnO nanostructures are generated. X-ray diffraction, transmission and scanning electron microscopy, Fourier transform infrared, and micro-Raman spectroscopy were all used to comprehensively examine both undoped and doped nanostructures.(1) Investigation using XRD allowed for the determination of the wurtzite phase as well as the lattice properties that correlate to it. Images obtained using scanning and transmission electron microscopy demonstrates that a change in the nickel doping level results in a transformation of the nanostructure of ZnO. It is possible that we will use FTIR and Raman spectroscopy to investigate the vibrational modes of nanostructures at various phases of structural change. This will allow us to gain a deeper comprehension of the crucial part that doping concentration plays in the gradual transformation of nickel-doped ZnO from nanoparticles to nanorods.

Process and Mechanism of Synthesis

According to a recent work by Goswami and colleagues, undoped and Ni-doped ZnO nanoparticles were produced via a straightforward chemical precipitation method. During the production process, powdered nickel oxide was used, which allowed for the incorporation of nickel (Ni) into zinc oxide (ZnO) at molar amounts ranging from 1% to 10%. All of the reactant chemicals were able to fulfil the conditions outlined below that were established by the American Chemical Society (ACS): $Zn(CH_3COO)_2.2H_2O$ (purity ≥ 98%); NaOH, NiO (black powder with a minimum purity of 99%). Zinc acetate solution was then mixed with a determined aliquot of NiO solution in order to achieve the necessary level of nickel doping concentration. Due to the fact that it is a base, a NaOH solution was added to this combination in a very measured manner. The sole technique of mixing that was used was magnetic stirring, and the end result was the precipitation of nanostructured Ni-doped ZnO. (2) Deionized water was used to remove any and all residues of pollutants that may have been present in the nickel-doped ZnO precipitate. After that, this precipitate was heated to 200 degrees Celsius and dried for six hours. The precipitate was first dried, then crushed up, and then annealed at a temperature of 400 degrees Celsius for two hours in order to eliminate carbonates and other impurities. After that, the Ni-doped ZnO is milled into a powder so that it may be used in later research. When it comes to chemical precipitation, the method and overarching strategy for the production of nanostructures may be found in another location. However, only the most important aspects of the method for producing Ni-doped ZnO nanoparticles are discussed in any detail here.

The following is an overview of the main chemical steps involved in the production of Ni-doped ZnO:

$$(1-x) \times [Zn(CH_3COO)_2] + x \times [NiO] + 2(1-x) \times [NaOH] \rightarrow Zn_{1-x}Ni_xO + 2(1-x) \times [CH_3COONa] + (1-x) \times [H_2O]$$

Nickel doping level is denoted by x in this context.

For Ni doping levels between 1% and 10%, our x values fall anywhere from 0.001% to 0.10%. When x is equal to 0.01, which corresponds to 1% Ni being doped into ZnO, the following is the balanced chemical process:

$$99[Zn(CH_3COO)_2] + [NiO] + 198[NaOH] \rightarrow Zn_{99}Ni_1O_{100} + 198[CH_3COONa] + 99[H_2O]$$

In order to calculate the Gibbs free energy of this reaction, we first utilise the same method as in the previous step, and then we

$(\Delta G_{reaction})$ **Using the relation:**

$$\Delta G_{reaction} = \Delta G_{products} - \Delta G_{reactants}$$

It is possible to determine the Gibbs free energy of formation if it is assumed that the typical temperature for preparing ZnNiO is 25 degrees Celsius (fG). When using a concentration of 1% of Ni-doped ZnO, it has been determined that the Gibbs free energy of reaction is -518.7 kJ/mol. This value was arrived at via calculations. This contradictory finding raises the possibility that ZnNiO nanostructures might form spontaneously, leading to an overall increase in energy. (3) Extensive research uses a variety of characterisation techniques to provide a comprehensive breakdown of the structural, vibrational, optical, and electrical features of the manufactured ZnO nanoparticles. (4)

X-Ray Diffraction Analysis

Spectra (a-e) in Figure 1 show the XRD -2 patterns of the powder samples recorded in the 2 range of 30o - 70o.

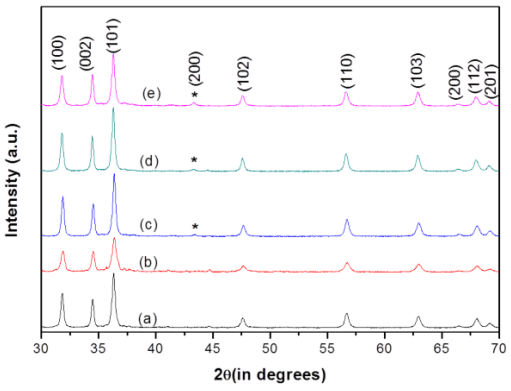

Figure 1: Schematics showing X-ray diffraction patterns for Ni doped ZnO nanostructures at concentrations of 1%, 3%, 5%, 7%, and 10%

Primary X-ray diffraction lines may be recognised as 31.8o, 34.6o, 36.3o, 47.6o, 56.7o, 62.9o, 66.4o, 68.0o, and 69.1o throughout all diffractograms. These lines correspond to reflections from the hexagonal wurtzite phase of ZnO. ZnO nanostructures with nickel doping display a second peak at 43.3 degrees, in contrast to the ZnO nanostructures without nickel doping, which show a peak at 43.3 degrees. The formation of NiO crystals, which is mostly driven by unsubstituted residual NiO, is denoted by the emergence of a peak at 43.3 degrees, which corresponds to the (200) plane of NiO. This peak shows the generation of NiO. The peak is more noticeable at 7 and 10 percent nickel concentration. When seen in this context, the situation is illuminated and makes sense. Because Ni atoms partially replace Zn atoms in the ZnO lattice, the XRD characteristic lines of 1% and 3% Ni-doped ZnO nanoparticles are comparable to those of undoped ZnO nanoparticles. This is due to the fact that Ni atoms are more electronegative than Zn atoms. It would seem that the wurtzite phase of ZnO is stable up to a replacement of Ni equal to 3%. After removing all other peaks from consideration, we are able to confirm that the synthesized nanostructures exclusively from the ZnNiO crystal phase, despite the presence of 3% Ni doping. The NiO (200) peak appears for the first time at a doping concentration of 5% Ni and is progressively more apparent as the Ni content of the sample increases. Since the (200) peak gets more prominent at higher doping concentrations, this demonstrates the presence of a NiO phase in addition to the ZnNiO phase. The formation of a second (200) peak at 5% Ni doping reveals that there is also a ZnNiO phase. (5)

There is no mobility in the XRD spectral lines seen in nanostructures containing 1-10% Ni dopant. This assertion is validated by the findings of the XRD study, which show that there will be no change in the values of the lattice constants. It was discovered that all nickel-doped ZnO nanostructures had the same lattice constants, which are a = 3.24 and c = 5.21 respectively. The average crystallite size of nickel-doped ZnO nanostructures is between 9 and 14 nm, in accordance with the Debye-Scherrer equation, with the exception of the 10% nickel-doped ZnO nanostructure, for which it is 28 nm. We decided to utilise microscopic characterisation so that we could see the structural change that was brought on by the considerable or little increase in crystallite size that was associated to the different doping doses.

Transmission Electron Microscopy (TEM) and Scanning Electron Microscopy (SEM) Analysis

Images obtained from transmission electron microscopy (TEM) and scanning electron microscopy (SEM) were analysed in order to determine the form, size, and size distribution of nickel-doped ZnO nanostructures ranging from 1-10% doping. (6)

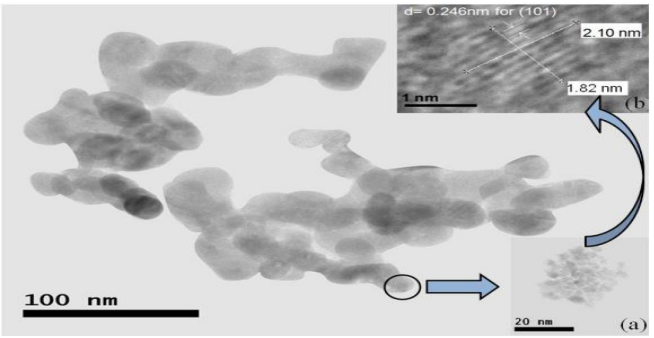

Figure 2: A transmission electron micrograph of nanoparticles of ZnO doped with 1% Ni.

It has been established that 1% nickel-doped ZnO nanoparticles have an average particle size of 20 nm, and this information is presented in Figure 2. Both the TEM picture (shown in Figure 4.2 as well as the inset an of Figure 2) and the HR-TEM image demonstrate that the 20 nm particles have been reduced in size to nanoparticles measuring 2 nm (inset b to Figure 2). The interplanar spacing of the nanoparticles, which measures 0.246 nm and is shown by the HR-TEM picture of the nanoparticles, which have a size of around 2 nm, corresponds to the (101) plane of ZnO. When nickel was introduced to ZnO nanostructures, transmission electron micrographs revealed the same effects as before. An analysis using X-ray diffraction showed that the lattice constants for all of the nickel doped ZnO nanostructures are a = 3.24, c = 5.21, and the d-spacing value is the same for all of the synthesised nanostructures. This value was found to be consistent across all of the nanostructures. (7)

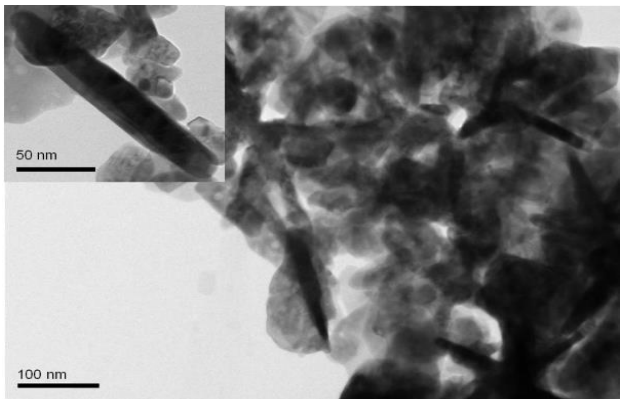

Figure 3: The TEM picture of 7% Ni doped ZnO nanostructures shows the formation of nanorods together with nanoparticles

At a doping level of 7% Ni, the creation of nanorods replaces the development of nanoparticles as seen in Figure 3. In addition to the synthesis of nanoparticles, the doping concentration of 7% Ni results in the manufacture of nanorods with dimensions of 25025 nm in length and 255 nm in width (see main and inset pictures of Figure 3).

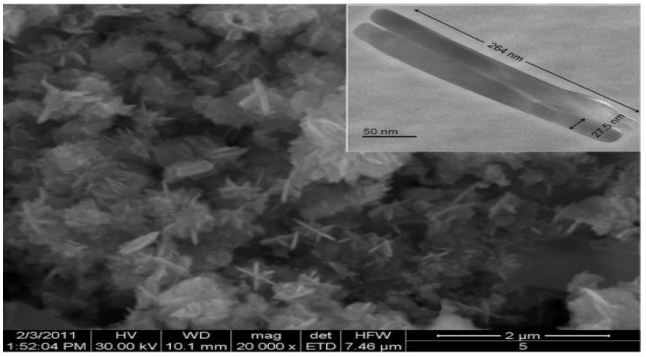

Figure 4: A scanning electron image of 10% nickel-doped ZnO shows how nanoparticles become nanorods completely

Last but not least, Figure 4 shows scanning electron micrographs and transmission electron micrographs of Ni-doped ZnO nanostructures at a concentration of 10%. It is clear that the nanoparticles underwent a structural change due to the fact that the SEM photo only reveals clusters of nanorods and none of the original nanoparticles have survived. The HR-TEM image that can be seen in the inset of Figure 4 reveals that the nanorods have a length of 264 nm and a thickness of 27.5 nm. Studies using X-ray diffraction reveal that zinc oxide only has a single wurtzite phase up to 3% nickel substitution. This finding is congruent with the nanoparticles that were discovered for zinc oxide that was doped with 1% and 3% nickel. However, when the doping level is at least 5% or higher, a new XRD peak for NiO (200) appears. Because Ni doping at 5 wt% or greater does not result in complete replacement inside the ZnO lattice, an additional NiO phase is formed in addition of the ZnNiO phase. The findings of x-ray diffraction and scanning electron microscopy have led us to the conclusion that the transformation of ZnO nanoparticles into nanorods is caused by the presence of Ni, which is doped into the material. When an excessive amount of Ni is doped into ZnNiO, nanorods are produced as a prelude to the material's future development in an anisotropic direction. (8)

Fourier Transforms Infrared (FTIR) Spectroscopy Analysis

It is essential to understand the surface chemistry of nanomaterials because atoms and molecules rapidly adsorb onto their surfaces rather than into their interiors. The Fourier transform infrared (FTIR) spectroscopy was used in order to quickly analyse the diverse vibrational modes in undoped and Ni doped ZnO nanostructures, as well as to determine the predicted variation in vibrational modes during different stages of structural transformation. The transmission FT-IR spectra of undoped ZnO nanoparticles as well as those with Ni doping. (9)

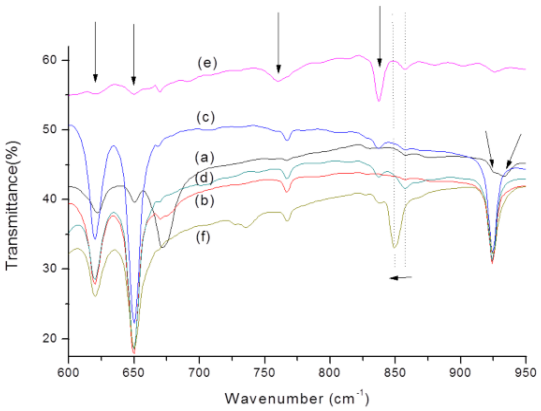

Figure 5: FTIR spectra of (a) undoped ZnO, (b) 1%, (c) 3%, (d) 5%, (e) 7% and (f) 10% of Ni doped ZnO nanostructures

In order to accurately identify the variations in the infrared spectra that are created by Ni doping, it is required to investigate the vibration modes that are caused by Zn-O bonding in both undoped and Ni doped ZnO nanostructures. Frequencies in the range ranging from 1000cm1 to 1mm1 are often the subject of research conducted by scientists who are seeking for evidence of infrared active bonding between inorganic components. Infrared absorptions characteristic of Zn-O vibrations can be seen in every one of the nanomaterial samples, and they can be seen at 620 cm-1, 653 cm-1, and 762 cm-1 (arrows in Figure 5). Because these modes are present, we may deduce that the ZnO phase has indeed crystallised in each and every one of the nanostructures. (10)

We examine the FTIR spectra of undoped and doped ZnO nanostructures in order to find out how the incorporation of Ni into ZnO nanostructures influences the structural alteration of the material. Only ZnO samples with a Ni doping percentage of less than 3% are able to display the infrared band located at around 837 cm-1. When the amount of Ni doping is increased, this mode is produced as a result of ZnO bond vibrations and defect state modes. When ZnO nanostructures are doped with nickel, new vibrational modes owing to Ni substitution should develop in addition of the Zn-O-Ni vibrational modes that appear at 3% Ni doping or higher. These new vibrational modes should emerge in addition to the Zn-O-Ni vibrational modes. This can be deduced from the observations of the doublet modes at 925 cm-1 and 933 cm-1 in undoped ZnO. (marked by two arrows in Figure 5). ZnO that has not been doped has a unique vibrational mode at 933 cm1. By detecting the shift or absence of the Zn-O-Ni vibrational mode in nickel-doped ZnO nanostructures, it is able to infer the defect state density that surrounds Ni ions. The 933 cm-1 mode is suppressed in nickel-doped ZnO nanostructures, but the 925 cm-1 mode is not affected by this doping. According to these observations, the doping of ZnO nanostructures with Ni alters the connection between Zn and O and, as a consequence of this, the vibrational modes.

We also discuss how the modification of the metal-oxygen vibrational modes that are already present in the material is brought about by the introduction of Ni doping into ZnO nanostructures. The peak that can be seen at 857 cm-1 is caused by Zn-O bonding, which is influenced by defect states. Because Zn-O bonding is present, all of the synthesised samples have a mode in their vibrational spectra that has a frequency of 848 cm-1. However, the position of this mode is red-shifted by 9 cm-1 in the sample that has 10% Ni doping. Because the transition from particles to rods is irreversible at that moment, this mode only appears when the Ni doping concentration is cranked up to its maximum value. The Zn-vibrational O mode changes to red when doped with 10% Ni, which indicates that the link between the atoms is weakened. Anisotropic development, which ultimately leads in the production of nanorods, is supported by the growing Ni content in ZnNiO nanostructures. This may lead to Ni-O interactions predominating in Zn-O-Ni links, which in turn encourages the formation of nanorods.

Important aspects of the material and its reaction to IR radiation may be inferred from the position and movement of peaks in the spectrum, in addition to the fluctuation in peak intensity, which can be used to draw conclusions about the material. To eliminate the possibility of a concentration-dependent relative fluctuation in the intensity of any IR mode in the synthesised nanomaterials, we obtained FTIR spectra of the samples while keeping a constant weight fraction in the KBr matrix. This allowed us to rule out a concentration-dependent relative fluctuation in the intensity of any IR mode. We have shown that the intensity of the basic Zn-O and ZnO-Ni modes shifts, depending on whether or not the ZnO nanostructures were doped with Ni at a concentration of 1-10%. The IR intensities of the Zn-O mode are at their lowest for 7% Ni doped ZnO between 620 and 653 cm-1, while the Zn-Ni-O mode has the greatest peak intensity at 837 cm-1. This is made clearly clear by the FTIR spectra of undoped and 1- 10% Ni-doped ZnO nanostructures. The fact that 7% Ni doped ZnO displayed the lowest and maximum IR intensity of the aforementioned modes provides further evidence that the synthesised nanostructures underwent structural change. Since the frequencies of identical vibrational modes are maintained in both undoped and Ni-doped ZnO nanostructures, we get to the conclusion that the structural modifications induced by Ni doping result in variations in the intensities of the different modes. At a ratio of 7% Ni:ZnO, a structural change from nanoparticles to nanorods takes place. This is most likely the cause of the lowest values of IR intensities of Zn-O modes (i.e. 620cm-1, 653cm-1) and the maximum value of IR intensity of Zn-O-Ni mode. A rearrangement of Zn-O/Zn-Ni-O bonds is one of the probable explanations for the observed drop in IR intensity that occurs in response to an increase in the concentration of Ni doping.

Micro-Raman Spectroscopy (μRS) Analysis

Using micro-Raman spectroscopy, the goal of this study was to figure out how the amount of nickel doping influenced the vibrational modes of nickel-doped zinc oxide at various stages in the development of the material's structure. Raman spectra provide the possibility of identifying crystallisation, structural disorder, and defects in micro and nanostructures. Wurtzite crystals, like ZnO, are an invaluable resource for the study of Raman spectroscopy when it comes to the investigation of basic physical processes. This is because of the crystals' easy uniaxial structures. The recording of Raman spectra in the range of 100 to 1200 cm-1 allowed for the study of the vibrational features of undoped and Ni-doped ZnO nanostructures, as well as the influence of doping on the nanostructures' microscopic structure, phase, and related parameters. A bar at the top of Fig. 6's plots a-f, which exhibit Raman spectra of undoped and 1-10% Ni doped ZnO nanostructures, respectively, displays the eleven Raman lines that are considered to be the most significant. These lines are numbered from one to eleven. (11)

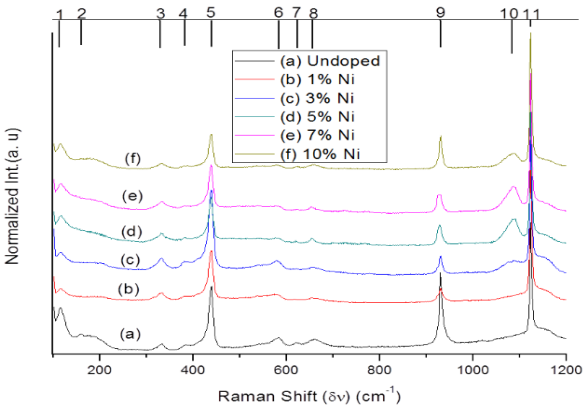

Figure 6: Micro-Raman spectra for undoped and 1-10% Ni doped ZnO nanostructures are shown in (a) through (f), respectively

The emergence of Raman modes in manufactured nanostructures in a sequential fashion. The mineral wurtzite, which is zinc oxide, has a crystal structure that resembles a formula unit primitive cell. This cell has the space group C46v, and all of the atoms are placed in the C3V sites (P63mc). The following collection of modes is obtained by a group theoretic study of the symmetry modes of the equivalent optical phonons at the centre of the zone: $A_1 + 2B_1 + E_1 + 2E_2$. The $A_1 + E_1 + 2E_2$ modes are Raman active, and 2B1 phonons don't make a sound. A1 and E1 modes may be further separated into their LO and TO sub-components. In the Raman spectra (Figure 4.6, a-f), characteristic modes at 115 (E2), 383 (A1), and 438 (E2) cm-1 have been identified and ascribed to low (E2), A1 (TO), and high (E2) modes, respectively, for both undoped and Ni-doped ZnO nanostructures. The low frequency E2 mode is associated with the non-polar vibration of the heavier Zn sub-lattice, whereas the high frequency E2 mode is caused by the displacements of the lighter oxygen atoms. All Raman spectra show a supplementary vibrational mode at around 580 cm1. ZnO's E1 (LO) mode (583cm-1) and A1 (LO) mode both reside here (574cm-1). Our XRD examination of both undoped and Ni-doped ZnO nanostructures confirms that the crystal phase of these materials is a hexagonal wurtzite, and the development of these basic Raman modes supports this conclusion.

Previous research shown that ZnNiO nanostructures maintain an excellent wurtzite structure of ZnO when the full width at half maximum (FWHM) of the E2 (high) mode is less than 11 cm-1. Although the E2 (high) mode expands with increased Ni presence, this indicates that the ZnO's wurtzite crystalline structure is degrading. As a result of our line shape study utilising Lorentzian fitting, we estimate that the FWHM for the E2 (high) mode is smaller than 11cm-1 in both undoped and 1-10% Ni doped ZnO nanostructures. This indicates that the hexagonal wurtzite crystalline structure of ZnO nanostructures remains unchanged by Ni doping at levels of 1-10%.(12)

After going over the fundamentals of ZnO's single phonon modes, we will now go over some of the extra modes that can be detected in the Raman spectra of undoped and Ni-doped ZnO nanostructures. The Raman band with a frequency of 930 cm-1 is often associated with the functional groups in glass. The Si-O bonds in esperite are stretched in an asymmetrical fashion, which is reflected in the mineral's Raman spectrum as a peak at 931 cm-1. This mode is present in each of our Raman spectra, which we obtained after characterising the materials after they had been deposited on a glass substrate.

CONCLUSION

The magnetic and semiconducting characteristics of individual nanoparticles in a system constituted of doped transition metals closely correspond with the system's overall properties. Clarifying other theoretical interpretations, such as spin correlation in DMS, relies heavily on this finding. With this theoretical knowledge, researchers and engineers might theoretically plan to perform experiments on semiconductor magnetic nanostructures and build devices with these materials. We decided to carefully investigate the characteristics of transition metal doped semiconductor nanostructures due to the importance of such studies.

REFERENCES

1. The Scale of Things - Nanometers and More, (2016, October 10), Office of Science, Department of Energy (DOE), United States Government

2. Sahai A., Goswami N., Kaushik S. D., Tripathi S., "Cu/Cu_2O/CuO Nanoparticles: Novel Synthesis by Exploding Wire

Technique and Extensive Characterization", Appl.Surf. Sci., vol. 390, pp. 974-983, 2016.

3. Wang Y., Lü Y., Zhan W., Xie Z., Kuang Q., and Zheng L., "Synthesis of porous Cu_2O/CuO cages using Cu-based metal–organic frameworks as templates and their gas-sensing properties", J. Mater. Chem. A, vol. 3, pp. 12796-12803, 2015.

4. Mishra M., Krishna T.C.S., Aggarwal N., Gupta G., "Surface chemistry and electronic structure of nonpolar and polar GaN films", Appl. Surf. Sci., vol. 345, pp. 440-447, 2015.

5. Mishra M., Krishna T. C. S., Kumar M., Gupta G., "Origin of surface electron accumulation and fermi level pinning in low energy ion induced InN/GaN heterostructure", Mater. Chem. Phys., vol.162, pp.640-644, 2015

6. Mishra M., Krishna T. C. S., Aggarwal N., Kaur M., Singh S., Gupta G., "Pit assisted oxygen chemisorption on GaN surfaces‖, Phys. Chem. Chem. Phys., vol. 17, pp. 15201, 2015.

7. Gang B. G., Varma M.R., and Santhosh P. N., "Evidence of reduced antiferromagnetic transition in mesocrystals of CuO synthesized by a surfactant-free solution phase method", Cryst. Eng. Comm., vol. 17, pp.7086-7093, 2015.

8. Srinet G, "Synthesis and Characteriazation of doped ZnO", Ph.D. Dissertation, Dept. Phys. Mat. Sci., Jaypee Institute of Informatiion Technology, Noida, U.P., 2015 [Online] Available: http://hdl.handle.net/10603/42983.

9. Su D., Xie X., Dou S., and Wang G., "CuO single crystal with exposed {001} facets - A highly efficient material for gas sensing and Li-ion battery applications", Scientific Reports, vol. 4, Article Number:5753, 2014.

10. Sahai A., Goswami N., "Structural and vibrational properties of ZnO nanoparticles synthesized by the chemical precipitation method", Phys. E, vol.58, pp.130-137, 2014.

11. Sahai A., Goswami N., "Probing the dominance of interstitial oxygen defects in ZnO nanoparticles through structural and optical characterizations", Ceramics International, vol. 40, pp. 14569–14578, 2014.

12. Martínez L., Kumar Y., Mayorga D., Goswami N., Agarwal V., "Labyrinth patternsof zinc oxide on porous silicon substrate", Superlattices and Microst., vol. 67, pp. 72- 81, 2014.

Corresponding Author

Deepak Chaurasiya*

Research Scholar, Shri Krishna University, Chhatarpur M.P.